Geomechanics and Engineering, *Vol. 40, No. 6 (2025) 395-410*
https://doi.org/10.12989/gae.2025.40.6.395

Evaluating the interaction between tunnel excavation and battered piles: Effects of depth and position using 3D numerical analysis

Mukhtiar Ali Soomro[1], Shaokai Xiong[1], Dildar Ali Mangnejo*[2], Hemu Karira[2] and Sharafat Ali Darban[1]

[1]*School of Mechanics and Civil Engineering, China University of Mining and Technology, Xuzhou, Jiangsu, P.R. China*
[2]*Department of Civil Engineering, Mehran University of Engineering and Technology, Shaheed Zulfiqar Ali Bhutto Campus, Khairpur Mir's, Sindh, Pakistan*

(*Received July 23, 2023, Revised February 22, 2025, Accepted February 27, 2025*)

Abstract. As urban areas continue to expand and densify, the demand for innovative transportation solutions, such as underground transit systems, has intensified. A critical consideration in such projects is the proximity of tunneling activities to existing infrastructure, particularly battered piles, which are widely used for their superior strength and ability to withstand lateral loads. Despite their importance, the effects of tunnel excavation on adjacent battered piles remain poorly understood. The research focuses on three critical tunnel depths: near the pile shaft, close to the pile toe, and below the pile toe. Additionally, it examines the position of the tunnel in relation to the batter of the pile, considering tunneling on the batter side, opposite the batter, and across the batter. Using an advanced numerical model simulating clay behavior, the study reveals that settlement and load transfer mechanisms of battered piles are significantly affected by tunnel position and pile embedment length. Key findings show that maximum settlement occurs when tunneling is near the pile and on the battered side, while the largest pile deflection is observed when tunneling occurs close to the pile shaft. The research also identifies a 'dragload' effect due to negative skin friction and induced bending moments when tunneling near the pile shaft. These insights are crucial for optimizing the design and performance of battered piles in tunnel projects, ensuring their resilience and minimizing risks to surrounding structures. The study contributes to a better understanding of soil-structure interaction in urban tunneling, providing valuable guidance for engineers and researchers.

Keywords: battered pile; *py* curves; stiff clay; settlement; tunnelling

1. Introduction

Rapid population growth and limited urban space have compelled engineers to develop more advanced and efficient transportation solutions. In response, underground transit systems have emerged as a critical focus of modern infrastructure development (Ding *et al*. 2017, Ye *et al.* 2023, Xu *et al.* 2024). However, the scarcity of available land in densely populated areas often necessitates the construction of these tunnels in close proximity to existing structures, such as high-rise buildings, bridges, and other critical infrastructure (Lu *et al.* 2020, Lee 2019, Karira *et al*. 2022, Xu *et al.* 2025a). This proximity introduces significant engineering challenges, including the need to mitigate potential impacts on adjacent structures and ensure the safety and stability of both new and existing systems. As a result, innovative design and construction techniques are essential to address these complexities and achieve sustainable urban development. Battered piles have historically been employed as a means of withstanding substantial lateral forces arising from wind, water waves, soil pressures for example I-10 Twin Span Bridge supported on battered pile groups (Souri *et al*. 2016, Bharathi *et al.* 2022, Soomro *et al*. 2024a, b). One notable feature of battered piles is their ability to transmit lateral loads by utilizing axial compression, in addition to shear and bending, which sets them apart from vertical piles. Nevertheless, due to the constraints of urban space, it becomes necessary to build these tunnels in close proximity to preexisting infrastructures. This proximity can lead to many adverse effects such as settlement, lateral displacement, and tilting of piled structures, hence posing a potential risk to the stability of the piled foundation. In a study conducted by Jacobsz *et al*. (2006), it was observed that a pair of tunnels, measuring 35 km in length, were built in close proximity to a bridge that was supported by both vertical and battered piles. The support system for each bridge pier consists of a collective sum of 31 piles, with 12 being oriented vertically and 19 inclined at a batter angle. The vertical piles were constructed using a driven-cast-in situ method, whilst the battered piles were created by a bored technique. Therefore, it is imperative to examine the effects of tunnelling on nearby battered piles. In this regard, theoretical analysis (Mu *et al.* 2021, Zhang *et al*. 2011), numerical simulation (Lee and Ng 2005, Lee 2013, Soomro *et al.* 2023, Soomro *et al.* 2022a, b, Gu *et al*. 2023a, b, Xu *et al*. 2025b), physical scale model test (Lu *et al.* 2020, Soomro *et al*. 2024b, Ng *et al*. 2015) and field test (Coutts and Wang 2000) are adopted by some researchers to discuss

*Corresponding author, PhD candidate
E-mail: dildarali@muetkhp.edu.pk

ISSN: 2005-307X (Print), 2092-6219 (Online)

the tunnel-soil-pile interaction. Among them, the deduction of the theoretical analysis method is excessively detailed, bringing an appearance of poor engineering applicability. Despite of several assumptions involved, the numerical modelling has high efficiency and low cost. The field test is subject to high cost and high risk (Meguid *et al*. 2008, Jamil *et al.* 2019). Considering the full-scale model test with difficult operability, so physical scale model test, as a method with superior cost performance, is frequently adopted (Loganathan *et al*. 2000). The physical scale model test consists of two categories, namely, single gravity (i.e., 1***g***) and multiple gravities (i.e., N***g*** under centrifugation conditions) model tests. 1g scale model test has a good economy, but the in-situ stress cannot be completely reproduced. Based on it, some scholars have indeed investigated the tunnel-soil-pile interaction by performing centrifugal scale model tests. By summarizing the current literature published, it is mainly divided into the following categories, namely, tunnel-sand/clay ground-single pile (Ng *et al*. 2013, Loganathan *et al*. 2000, Lee and Chiang 2007, Ng and Lu 2014), tunnel-sand/clay ground-pile group (Ng *et al.* 2014, Loganathan *et al*. 2000, Soomro *et al.* 2020, Hong *et al*. 2015, Franza and Marshall 2018, 2021a, b, Boonsiri and Takemura 2015, Zhang *et al.* 2011), tunnel-sand/clay ground-piled raft interaction (Lu *et al*. 2020). These investigations have demonstrated that extent of tunnelling-induced settlements is notably influenced by factors such as tunnel volume loss and tunnel depth at which the tunnel is buried relative to the piles.

A considerable amount of prior research has been dedicated to understanding the behaviour of vertical piles in response to tunnel excavation. However, the potential effects of tunnelling on nearby battered piled foundations, specifically in terms of three-dimensional consequences, have yet to be well investigated. This study seeks to comprehensively examine the settlement and load transfer mechanism of a pre-existing battered single pile caused by a tunnel in clay. In order to accomplish these objectives, this paper conducts a parametric investigation using a three-dimensional coupled-consolidation numerical approach. The study presents and examines several aspects related to the settlement and deflection of battered piles, including *py* curves, axial load distribution along the pile, stress variations, and bending moment throughout the development of tunnelling operations.

2. Development of three-dimensional numerical model

2.1 Description of geometry of the numerical models

The present study investigates effects of advancing tunnel on an existing battered pile in medium stiff clay. To achieve this, numerical analyses are conducted using the three-dimensional finite element program Abaqus 6.14-2 (Hibbitt *et al*. 2015). The analysis takes into account the soil consolidation that occurs during tunnel construction through the implementation of coupled-consolidation analysis. The study investigates two factors: the depth of the tunnel in relation to length of pile, and location of tunnel in relation to batter of the pile. Three critical depths along the pile depths are selected which are near pile shaft (S), close to pile toe (T) and below piles toe (B). Furthermore, this study also considers the positioning of tunnel in relation to the pile's batter. The tunnel can be located at the batter side (the inclined portion of the pile) (b), opposite the batter (o), or across the batter (a). The cases are denoted according to tunnel location relative to pile length and batter of the pile e.g., S_b represents the case in which tunnel is excavated near pile shaft and batter side of pile. Figs. 1(a)-1(c) depict the elevation view of cases S_b, S_o, and S_a, respectively. In the scenario of S_b, the simulation of tunnelling occurs in close proximity to the adjacent pile shaft and on the batter side of the pile. In contrast, in the S_o and S_a scenarios, the tunnel is excavated on the opposite side of the pile batter, and it extends across the pile batter. In this study, the tunnel diameter is taken as 6 m (*D*), while the cover is measured at 8 m *(C*). Consequently, the cover-to-diameter ratio (*C/D*) of the tunnel is determined to be 1.33. The present study investigates the embedded length (L_p) and diameter (d_p) of a pile, which are measured to be 18 m and 0.8 m, respectively. The pile is inclined at a batter angle (θ) of 20°, which is the optimized angle for the battered pile (Bharathi *et al*. 2022). A working load in vertical direction is applied on the battered pile head. The determination of the magnitude of the vertical working load is achieved by a numerical pile load test, as detailed in section 2.4. The distance (*s*) separating the tunnel and the battered pile is 2.5 m, which is equivalent to 0.42 times the diameter (*D*). Similarly, Figs. 2(a)-2(c) depict elevation view of three cases: T_b, T_o, and T_a. The dimensions of the tunnel diameter, pile diameter, embedded length, pile and clear space between the tunnel and the pile are consistent with the values depicted in Fig. 1. The sole differentiation is in depth of the tunnel in relation to the pile. In the scenarios of T_a, T_o, and T_a, the tunnel excavation is conducted adjacent to the pile toe, with a cover-to-diameter ratio (*C/D*) of the tunnel being 2.33. The cases where tunnel is excavated below the battered pile toe, referred as B_b, B_o, and B_a, are represented in Figs. 3(a)-3(c), respectively. In each case, the ratio of the cover-to-diameter (*C/D*) of the tunnel is taken 3.53. In addition, three numerical simulations are modelled in which tunnelling effects on vertical pile are investigated. Figs. 4(a)-4(c) shows elevation views of cases S_v, T_v and B_v, respectively. The tunnel is excavated near pile shaft of the vertical pile, next to and below the vertical pile toe in cases of cases S_v, T_v and B_v, respectively. The tunnel in the simulation has a length of 72 m, which corresponds to 12 times the diameter the tunnel. The simulation of the excavation process for each tunnel was conducted in 28 discrete steps. In accordance with the findings of Lee (2013) and Lee and Ng (2005), the tunnel progressed by a magnitude of 2.5 m (0.42 times the diameter, *D*) during each individual stage. A time increment of one day was employed for each step in the finite element analysis. In order to monitor the development of the tunnel advances, a monitoring section positioned at the transverse centerline of the pile (namely, $y/D = 0$) was chosen as a point of reference.

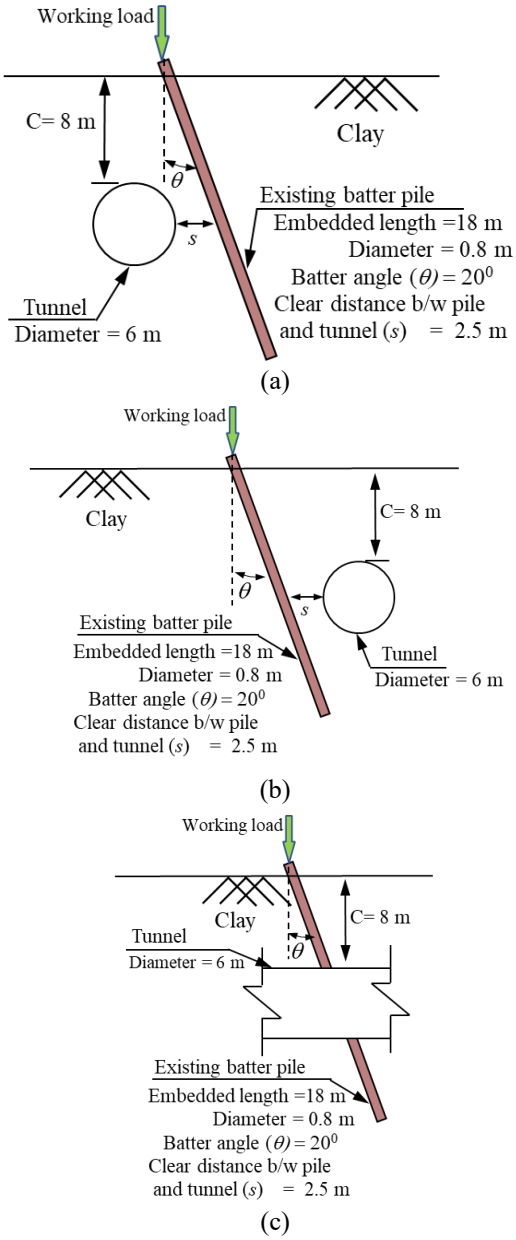

Fig. 1 Elevation view of numerical simulations of cases (a) S_b, (b) S_o; and (c) S_a

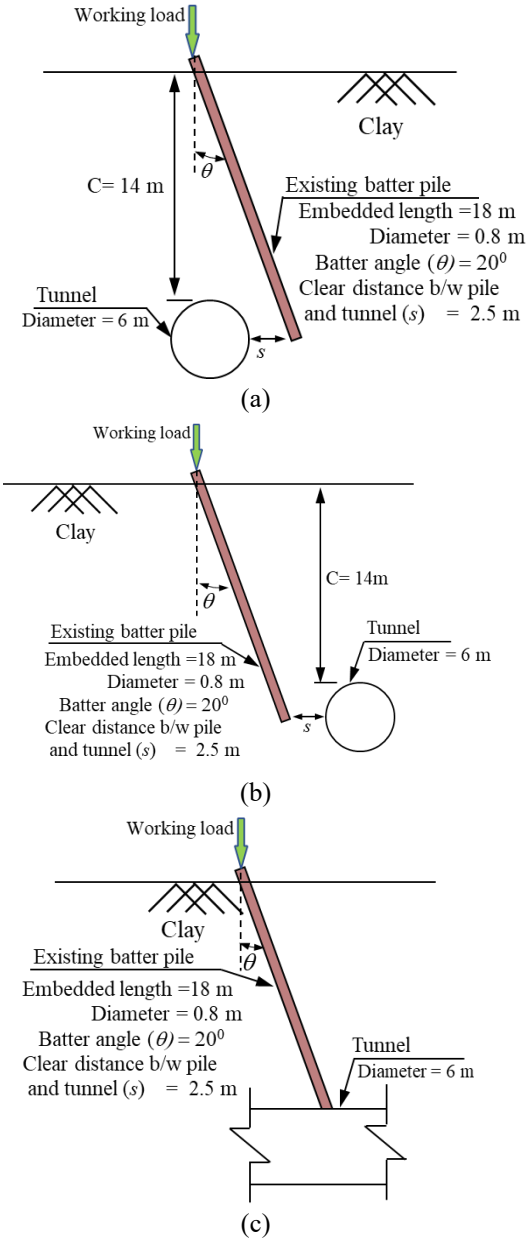

Fig. 2. Elevation view of numerical simulations of cases (a) T_b, (b) T_o; and (c) T_a

The primary objective of this study is to examine the effects of tunnelling on a battered pile under vertical working load. The magnitude of the vertical load, which is 1067 kN, was obtained from Soomro *et al*. (2023). They conducted a numerical pile load test to determine the ultimate load. After the ultimate capacity is determined from the pile load test, the working load is calculated by applying a factor of safety of 3.0 (Lu *et al*. 2020). This ensures a sufficient margin of safety in the design (Shi *et al*. 2019). The working load is subsequently applied to the battered pile in the succeeding numerical simulations. Table 1 presents a summary of the numerical simulations conducted.

2.2 Geometry discretisation, boundary and initial conditions

The primary objective of the study was to utilize three-dimensional finite element models to accurately represent the behaviour of battered piles in reaction to the presence of an advancing tunnel in close proximity. Fig. 5 depicts an isometric representation of a standard finite element mesh for the scenario denoted as S_bt. The dimensions of the mesh are as the length along the *y-axis* is 80 m, the width along the *x-axis* is 80 m, and the depth along the *z*-axis is 60 m.

The selection of depth of the model is determined to be ten times the diameter of the tunnel. The mesh is composed of 88,752 elements and 100,145 nodes. The solid element with 8-node brick, trilinear displacement, trilinear pore pressure (C3D8P) was used to model soil. The pile is discretized using 8-node linear brick. Coupled-consolidation analysis was performed to simulate

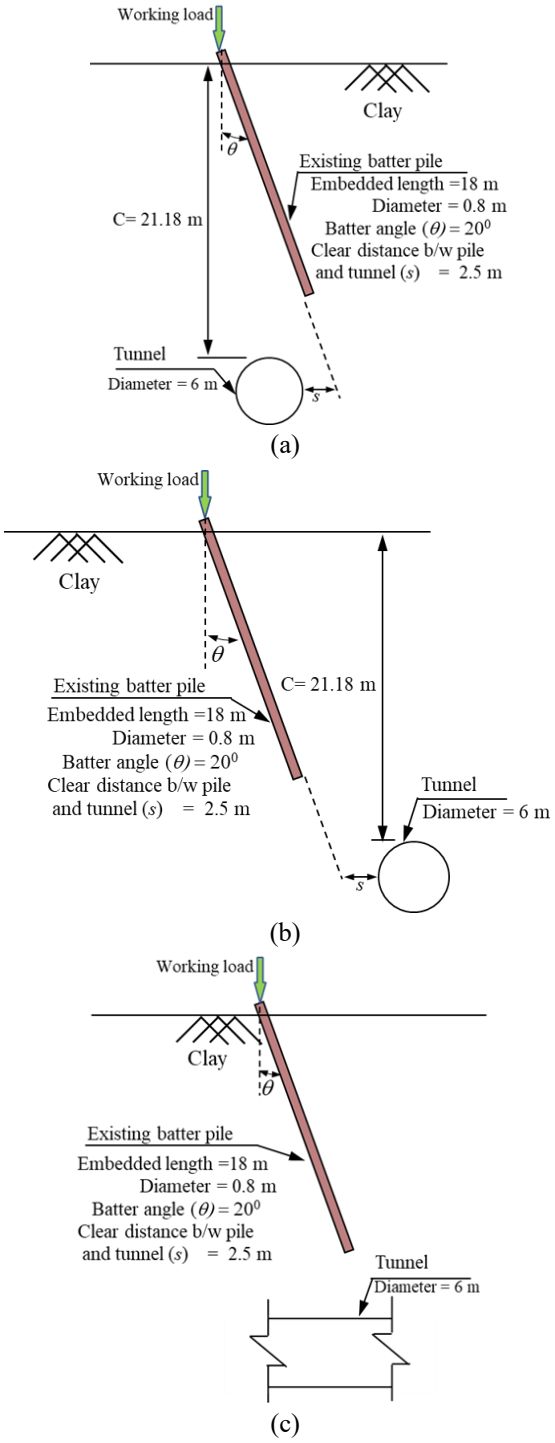

Fig. 3 Elevation view of numerical simulations of cases (a) S_b; (b) S_o; and (c) S_a

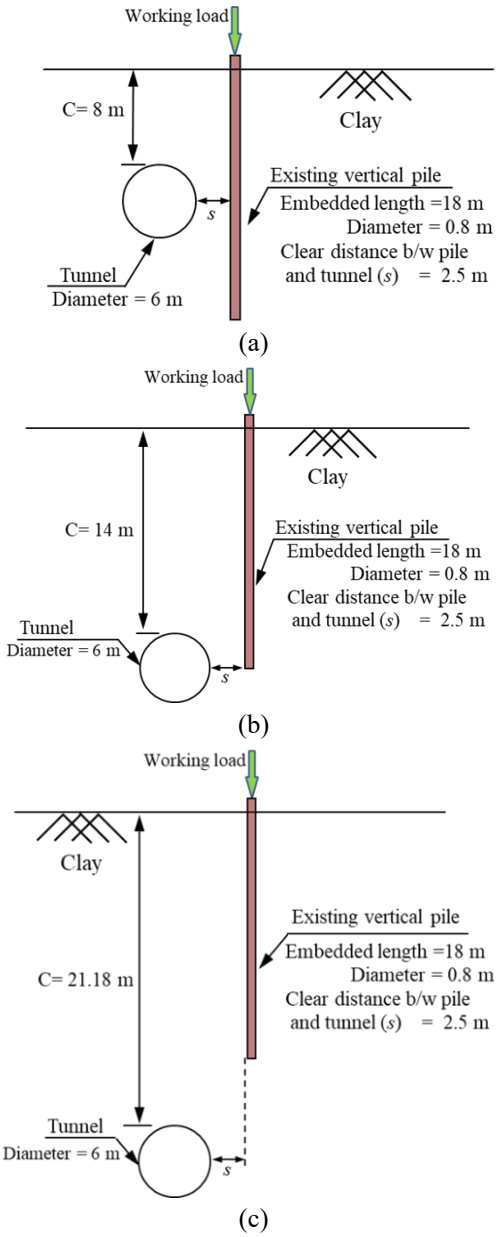

Fig. 4 Elevation view of numerical simulations of cases (a) T_b, (b) T_o; and (c) T_a

accumulation of excess pore water pressure. The sensitivity of the numerical results with respect to size of mesh was explored and it was found that without undermining stability of analysis, the optimum value 1.5 mm of element was chosen. The pile is discretized using an 8-node linear brick element. At the base of the mesh, all displacement components were set to zero, whereas only displacements perpendicular to the boundaries were constrained on the vertical sides. The geostatic (*in-situ*) stresses were initialized by using a saturated bulk unit weight of 16.5 kN/m^3 and a hydrostatic pore pressure distribution along the depth of the model with K_o value. Once equilibrium was achieved, the elements representing pile group were activated in soil mesh. Subsequently, lateral load (either towards or away from the tunnel) was applied on the top of pile cap. After stabilisation of effective stresses because of consolidation in the response of application of the load, the tunnelling was excavated. The present study employed the displacement-controlled model (DCM) according to the methodology introduced by Cheng *et al*. (2007). The determination of volume loss prior to the tunnelling operation involved establishing the dimensions of the gap between the tunnel lining and the excavated soil. The process known as "element death" was utilized to eliminate the soil in the specified location (Qian *et al*. 2020).

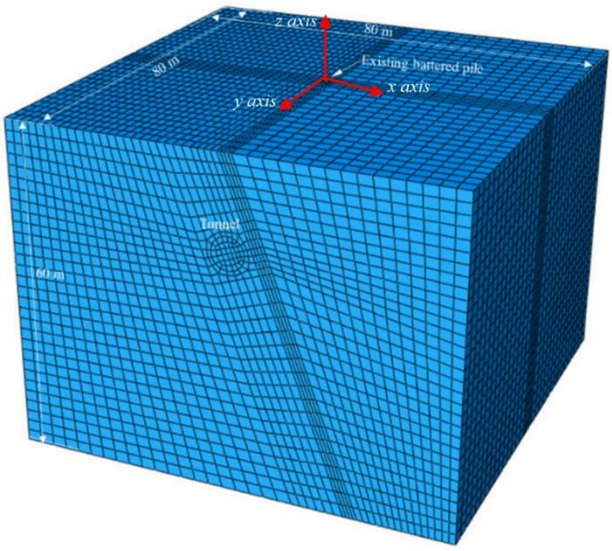

Fig. 5 Finite element mesh of a typical numerical analysis for the case of T_b

Table 1 Summary of numerical simulations

Case ID	*C/D*	Remarks
S_b	1.33	Tunnelling near pile shaft and battered side of the pile
S_o		Tunnelling near pile shaft and opposite side of batter pile
T_a		Tunnelling near pile shaft and across of batter pile
T_b	2.33	Tunnelling next to pile toe and battered side of the pile
T_o		Tunnelling next to pile toe and opposite side of batter pile
T_a		Tunnelling next to pile toe and across of batter pile
B_b	3.53	Tunnelling below pile toe and battered side of the pile
B_o		Tunnelling below pile toe and opposite side of batter pile
B_a		Tunnelling below pile toe and across of batter pile

Note: *C/D* = cover to diameter of tunnel ratio

Concurrently, the shell elements that represents the tunnel lining were activated. According to the findings of Mair and Taylor (1997), the utilization of earth pressure balance shields for tunnel excavation led to volume losses of around 1% in sand, whereas soft clay experienced volume losses of approximately 2%. Moreover, Abrams (2007) and Shirlaw *et al*. (2003) documented a range of volume losses between 1% and 4% in mixed-face tunnelling situations that encompassed both clay and sand materials. In this hypothesized investigation, a volume loss of 2% was implemented based on the information provided in these reports. In this study, the numerical model simulates a non-displacement pile, which closely resembles bored piles commonly used in practice. The installation effects were not explicitly modelled; however, the initial stress state around the pile was carefully established to reflect realistic in situ conditions. Since bored piles are formed by excavation and subsequent concrete placement, they do not induce significant radial soil displacement during installation, making them appropriate for the numerical representation used in this study. This approach ensures that the initial stress distribution in the numerical model is consistent with the expected field conditions for non-displacement piles. To consider the interaction between structures and soil, specific properties related to tangential behaviour and normal behaviour are chosen for the contact between the piles and soil. The Coulomb Friction model is utilized to define frictional contact properties, enabling the simulation of tangential behaviour. On the other hand, the Hard Contact model is employed to replicate the nature of surface contact and simulate normal behaviour in Abaqus. In all analyses, a standard value of μ (coefficient of friction) for a bored pile was assumed to be 0.35 (Tsubakihara and Kishida 1993, Shi *et al*. 2019b). To achieve complete mobilization of interface friction, a limiting shear displacement of 5 mm is considered. This approach is implemented consistently throughout the analyses.

2.3 Constitutive models and input Parameters

The application of a hypoplastic (clay) model has been utilized in order to effectively depict the characteristics of soil, including its capacity to replicate small strain stiffness (Mašin 2005). The primary objective of formulating the fundamental hypoplastic model was to provide a comprehensive representation of the nonlinear behaviour displayed by granular materials under conditions of moderate to large strain during monotonic loading (Mašín

Table 2 Model parameters of kaolin clay adopted in the parametric study

Description	Parameters
Effective angle of shearing resistance at critical state: ϕ'	22°
Parameter controlling the slope of the isotropic normal compression line in the ln(1 + e) versus lnp plane, λ^*	0.11
Parameter controlling the slope of the isotropic normal compression line in the ln(1 + e) versus lnp plane, κ^*	0.026
Parameter controlling the position of the isotropic normal compression line in the ln(1 +e)–lnp plane, N	1.36
Parameter controlling the shear stiffness at medium- to large- strain levels, r	0.65
Parameter controlling initial shear modulus upon 180° strain path reversal, m_R	14
Parameter controlling initial shear modulus upon 90° strain path reversal, m_T	11
Size of elastic range, R	1×10^{-5}
Parameter controlling the rate of degradation of the stiffness with strain, $_r$	0.1
Parameter controlling degradation rate of stiffness with strain,	0.7
Initial void ratio, e	1.05
Dry density (kg/m^3)	1136
Coefficient of permeability, k (m/s)	1×10^{-9}

and Herle 2005, Mašín 2005). The model consists of five parameters, namely *N, λ*, κ*, φc*, and *r*. The parameters *N* and *λ** determine the position and slope of the isotropic normal compression line in the ln(1+e) vs ln(*p'*) plane. Within this particular context, the symbol "*e*" is utilized to denote the void ratio, while the symbol "*p*'" is to symbolize the mean effective stress. The parameter *κ** is employed to represent the gradient of the isotropic unloading line inside the same plane. The critical state friction angle is represented by the symbol φ_c, while the parameter *r* controls the shear modulus in situations involving substantial strain. Niemunis and Herle (1997) proposed modifications to the fundamental hypoplastic model by incorporating the concept of intergranular strain. This addition was intended to address the strain dependency and route dependency of soil stiffness at small stresses. The enhancement of the system requires the incorporation of five additional factors, namely *R, β_r, χ, m_T, and m_R*. The parameter R is responsible for setting the amplitude of the elastic range, while β_r and χ determine the rate at which stiffness decreases. The initial shear modulus is determined by the parameters m_T and m_R when the strain path is reversed by 180° and 90°, respectively. The integration of the hypoplastic clay model, which incorporates modest strain stiffness, has been achieved within the Abaqus software program through the implementation of a user-defined subroutine. For the purposes of this hypothetical investigation, the selection of kaolin clay as the artificial soil was based on its well-documented geotechnical characteristics and physical features. The selection of kaolin clay is substantiated by previous scholarly investigations that have primarily examined the characteristics of its microstructure (Gasparre 2005), as well as conducted experiments related to seepage, compression, and shear (Benz 2007). Furthermore, the large literature has documented the widespread use of kaolin clay as a typical testing material in model studies that aim to replicate various soil-pile interaction problems (Loganathan *et al.* 2000, Wang *et al*. 2015). The parameters employed in this study for the hypoplastic clay model have been drawn from previous research conducted by Soomro *et al.* (2023). They calibrated and validated the hypoplastic clay model with the measured results from a centrifuge test performed by Loganathan *et al*. (2000). Additionally, the researchers provided evidence for their parameters by a comparative study, comparing the observed outcomes of cyclic pile behaviour in centrifuge studies. Table 2 presents a complete overview of the model parameters for clay and concrete. On other hand, the concrete pile was modelled using Hook's law as an elastic material with Young's Modulus, E=35 GPa and Poisson's ratio, $\nu = 0.3$.

3. Interpretation of computed results

3.1 Progressive pile settlement due to advancement of tunnelling

Fig. 6(a) presents a comparison of the settlement induced in a battered pile during the construction of a tunnel close to the pile shaft, considering three different scenarios: S_b, S_o, and S_a. The illustration includes the incremental settlement of the vertical pile caused by tunnelling, referred to as case S_v, for comparison. The settlement induced in a pile, denoted as S_p, is quantified as a percentage of the pile diameter, represented by d_p. The passage of tunnel is represented by normalised distance by tunnel diameter (*y/D*) which is measured from monitoring section.

The figure illustrates that in all four scenarios, when the tunnel is located at a sufficient distance from the pile (namely, at the monitoring portion where the ratio of *y* to *D* is equal to zero), no settlement is observed. Nevertheless, when the tunnel face is located at a distance of *y/D*=-4.0 behind the pile in scenarios S_b and S_o, the battered pile starts to undergo settlement. The induced settlement further increases as tunnelling activity is carried out closer to the pile. However, no substantial settlement was observed when the tunnelling activity is carried out at a distance of *y/D*=+4.0 both in front of and beyond the pile. Thus, the zone of influence was identified as being between *y/D*=-4.0

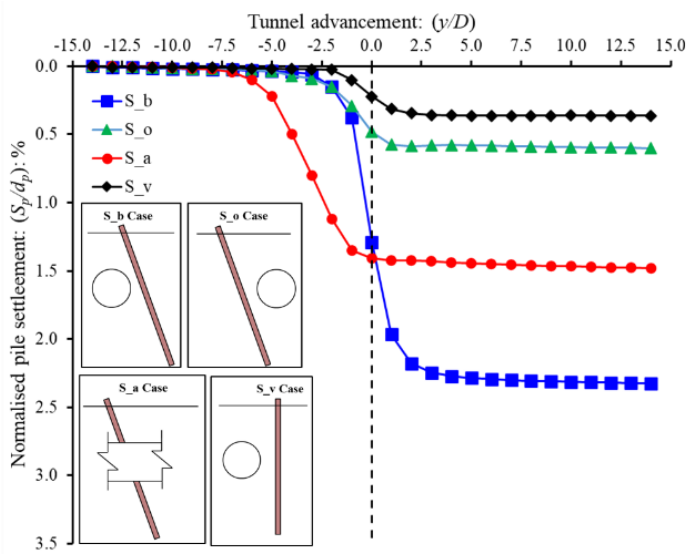

(a)

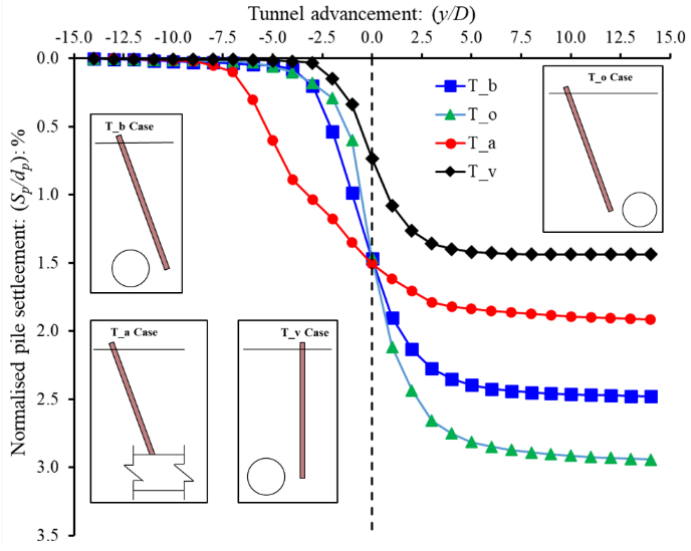

(b)

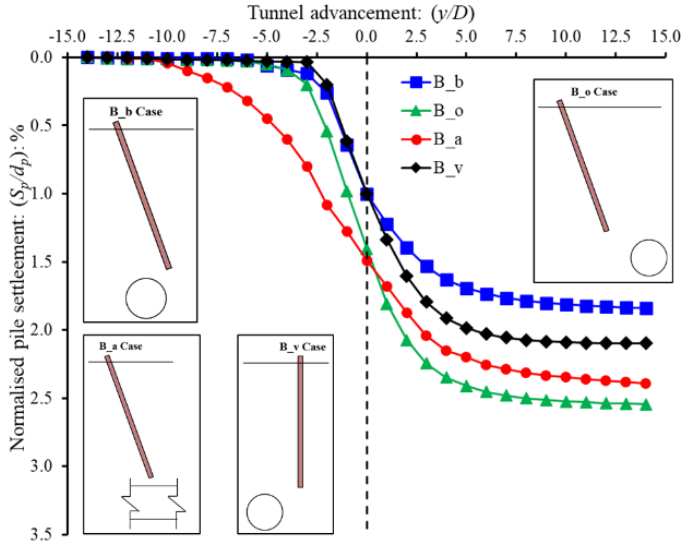

(c)

Fig. 6 Induced settlement of battered pile with tunnel advancement at (a) near pile shaft, (b) next to the pile toe; and (c) below the pile toe

and y/D=+4.0 in cases S_b and S_o. In contrast, for case S_a, the zone of influence (-7.0 ≤y/D≤+1.5) is larger than that observed in cases S_b and S_o. This can be because of the reason that the stress regime generated at the battered side of pile. The battered pile is influenced by the tunnel activity even if the tunnel face is farther from the pile S_a scenario. Compared to battered pile cases (i.e., S_b, S_o and S_a), the influence zone is smaller in vertical pile case (i.e., case S_v). This is attributed to the stress regime generated in the ground under the batter pile. Therefore, the battered pile started to settle with tunnel face farthest from the monitoring section in case of S_a. It was further observed that the maximum settlement was induced in the battered pile when the tunnel excavation is carried out at the battered side of the pile in case of S_b. This is because when tunnel activity is carried out at the battered side of pile, the tunnelling-induced ground movement towards the tunnel and the vertical component of the applied load pull the pile down as well. Due to this coupled phenomenon, the largest settlement was induced in the battered pile for case S_b. Conversely, tunnelling on the opposing side of battered pile for scenario S_o yielded the most minimal settlement of the battered pile. When comparing the tunnelling-induced settlements of battered and vertical piles, the tunnelling causes the least settlement of a vertical pile for case S_v. The computed results of this study have revealed that tunnelling activity near the pile shaft of a battered pile is more vulnerable than that adjacent to a vertical pile. The final induced settlement of 2.32%d_p, 0.60%d_p, 1.48%d_p and 0.36%d_p computed in cases of S_b, S_o, S_a and S_v respectively.

Fig. 6(b) depicts the settlement induced in the battered pile as a result of tunnel constructing adjacent to the pile toe, specifically in scenarios T_b, T_o, and T_a. The figure shown includes the incremental settlement of the vertical pile caused by tunnelling, referred to as case T_v. The data presented in the figure demonstrates that the settlement reaction of the pile subjected to tunnel advancement was comparable between the T_b, T_o, and T_a cases, as well as the S_b, S_o, and S_a cases. For scenarios of T_b, T_o and T_a, the zone of the influence of tunnelling on the battered pile was discovered as -4.0≤y/D≤+4.0. However, a wider zone of influence (which is -7.0≤y/D≤+5.0) was identified when the tunnel passes the pile across the battered position in case of T_a. The reason for this is attributable to the stress regime generated on battered side of the pile. When tunnel approaches to next of the pile toe, the stress regime is affected even if the tunnel face is at farther away from the battered pile. Furthermore, maximum settlement was induced in the battered pile when the tunnel was excavated on opposite of battered pile in case of T_o. This observation is different from that was made when tunnel passes near the pile shaft. This is because the lower part of the pile including the pile toe is substantially affected by the stress relief due to tunnelling next to the pile toe in case of T_o (discussed in section 3.4.2). Similar to the induced settlement due to tunnelling near the pile shaft, the induced settlement of vertical pile due to tunnelling in case of T_v is smaller that of the battered pile. The amount of the settlement of 2.50%d_p, 2.94%d_p, 1.91%d_p and 1.44%d_p were induced in the pile after tunnelling in cases of T_b, T_o, T_a and T_v, respectively.

Fig. 6(c) shows the induced pile settlement due to tunnelling which was excavated below the battered pile toe in cases of B_b, B_o and B_a. The incremental settlement of the vertical pile due to tunnelling (i.e., case B_v) is included in the figure for reference. Similar to the cases of tunnelling advancement near pile shaft and next to the pile toe, the zone of influence of tunnelling below the pile toe on the battered pile (cases B_b, B_o and B_a) is larger than that for the vertical pile case (i.e., case B_v). the influence zone (which is -10.0 ≤y/D≤+10.0) for the case of tunnelling across the battered pile (i.e., case B_a) is the largest among the battered pile cases. This observation can be ascribed to the stresses generated in the ground surrounded the battered pile. It is found that induced settlement of the battered pile due to tunnelling below the toe and other side of the batter in case of B_o is the largest among all the cases of tunnelling below the pile toe. This observation presents a contrasting perspective to intuition which is battered pile in case of B_b would settle larger than that in case of B_o.

The reason for this phenomenon is that the pile toe and the lower segment of the battered pile subjected to stress relief due to tunnelling, as explained in section 3.4.2. The aforementioned factor resulted in a decrease in the mobilized end-bearing capacity of the pile, as elaborated upon in section 3.7.1. In order to mobilize shaft resistance, it is necessary for the battered pile to undergo a settling process. As a result of the settlement of the battered pile, there was an increase in stresses seen at the top portion of the pile, as detailed in section 3.4.2. The settlement of the vertical pile resulting from the tunnel's advancement beneath the pile toe (referred to as case B_v) is comparatively smaller than the settlement induced in the battered pile in cases B_o and B_a. Nevertheless, the settlement caused by the battered pile in scenario B_b is smaller when compared to the settlement observed in the case of a vertical pile. Owing to arching at the crown of the tunnel, the stresses in soil around the entire pile increases (discussed in section 3.4.2) and resulted into mobiles shaft resistance. The final induced settlement of 1.84%d_p, 2.54%d_p, 2.40%d_p and 2.10%d_p computed in cases of B_b, B_o, B_a and B_v, respectively.

3.3 Load transfer mechanism along the battered and vertical piles due to advancement of the tunnelling

3.3.1 Changes in load distribution along the length of the pile

As discussed in previous section, the vertical working load applied on the battered pile head is resolved into two components (i.e., one normal to the pile and the other in the axial direction). In this section changes in load in axial direction along the length of the battered pile due to tunnelling is explored.

Fig. 7(a) presents a comparison of the axial load distribution along the length of both the battered pile and the vertical pile. This comparison is made before and after the excavation of the tunnelling near the pile shaft in

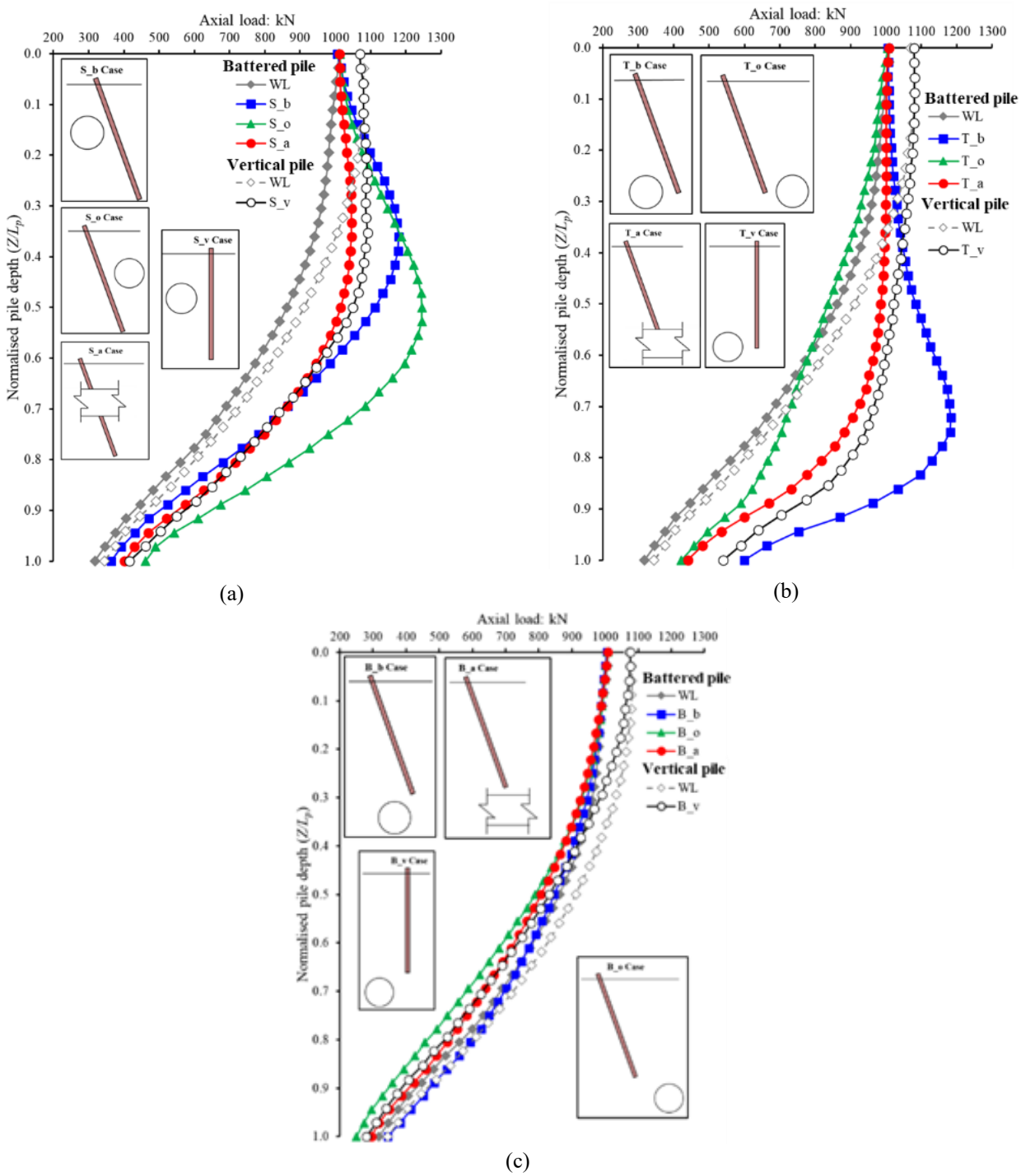

Fig. 7 Changes in axial load along the pile length (a) near pile shaft, (b) next to the pile toe; and (c) below the pile toe

scenarios S_b, S_o, and S_a. The axial component (i.e., 1010 kN) of the vertical working load (i.e., 1070 kN) was carried is carried by the battered pile as well as the vertical pile through a combination of 70% with shaft resistance and remainder 30% with end-bearing of the pile. In scenarios S_b and S_o, the upper section of the battered pile experiences a "dragload" as a result of the mobilization of negative skin friction upon the tunnel's completion. Nevertheless, the resistance experienced by the shaft at the upper portion of the vertical pile (Z/L_p<0.42) diminishes to a value of zero. The reason for this phenomenon is attributed to the fact that the pile shaft, which has been subjected to stress release, is a result of tunnelling activities, as elaborated in section 3.4.2. The inclined installation of the battered piles led to soil settlement that exceeded that of the pile. Consequently, the downward movement of the battered pile resulted in the occurrence of negative shaft resistance along its length. To maintain the equilibrium of the pile, it is necessary to activate positive skin friction (PSF) at the lowest section of the pile as well as to mobilize

end-bearing resistance. Upon the completion of the tunnel, the mobilized shaft resistance and end-bearing values exhibit an increase of 18% and 15% for the S_b case, and 9% and 28% for the S_o case, respectively. Due to the vertical orientation of the pile for S_v, the occurrence of stress release during tunnelling leads to limited movement between the pile and the soil. Consequently, the shaft resistance exerted on the upper part of the pile is considered negligible. Nevertheless, the axial load behaviour of the battered pile when subjected to S_a is comparable to that of a vertical pile. The excavation of the tunnel is conducted along the battered surface of the pile. Consequently, the settlement of battered piles generated by tunnel excavation is greater in magnitude compared to that of vertical piles, as illustrated in Fig. 6.

Fig. 7(b) illustrates the axial load distribution in both battered pile (T_b, T_o, T_a) and vertical pile (T_v) scenarios, before and after tunnelling. As a result of tunnelling adjacent to the pile toe in the case of T_b, there was an observed increase in axial load along the lower section of the pile (Z/L_p<0.30). The observed phenomenon can be attributed to a decrease in shaft resistance, which can be attributed to the release of stress induced by the tunnelling activity. The mobilization of negative shaft resistance occurs within the intermediate section of the pile, within the range of 0.50 to 0.75 relative to the pile length. Consequently, the aforementioned section of the battered pile experiences the drag load. In order to maintain the equilibrium of the pile, positive shaft resistance at the lower section was mobilised (Z/L_p>0.75) and also end-bearing of the pile. Upon the completion of the tunnel construction, the mobilized shaft resistance exhibited a rise of 85%, while the end-bearing had a 90% increase. In contrast, the resistance in the lower region of the pile is reduced in the case of T_o as a result of stress release caused by tunnelling. In order to counterbalance the decrease in shaft resistance, the settlement of the pile, as depicted in Fig. 6, mobilize both the shaft resistance and the end-bearing of the pile. Conversely, in the case of T_v, when tunnelling takes place near to the vertical pile toe, the axial load experienced an increase along the pile within depths ranging from 0.26 to 1.0 L_p. The increase in axial load can be attributed to a decrease in shaft resistance, which can be attributed to the stress release resulting from tunnelling activities in adjacent to the pile toe. Nevertheless, the axial load behaviour of the battered pile under the influence of T_a has similarities to that of a vertical pile. The reason for this is that the tunnel is excavated across the battered of the pile. Hence, the settlement induced by tunnel excavation is greater for a battered pile compared to a vertical pile, as depicted in Fig. 6.

Fig. 7(c) presents a comparison of the axial load distribution in the scenarios of battered piles (B_b, B_o, B_a) and vertical piles (B_v) before and after tunnelling. The figure illustrates that there is a slight variation in the axial load distribution over the length of the pile when considering the B_b scenario. The reason for this might be ascribed to the positioning of the tunnel, which is excavated below the pile toe. The soil movement generated by tunnelling exerts a drag on the battered pile, resulting in the settlement of the pile. The tunnelling-induced soil movement drag the battered pile causing the settlement of the pile. In contrast, the axial load exhibited a decrease along the battered pile length in the scenario of B_o. The observed decrease in end-bearing of the pile can be attributed to the presence of the tunnel, which induces stress release. In order to counteract the reduction in end-bearing resistance, the pile to undergo significant settlement (refer to Fig. 6) in order to mobilize the shaft resistance along the whole length of the pile. Tunnelling results in a 21% reduction in end-bearing capacity and a 10% increase in shaft resistance. The phenomenon of tunnelling in the case of B_a results in a decrease in the axial load experienced by the battered pile. The end-bearing resistance of a vertical pile (B_v) experiences a notable reduction. The batter pile settled in order to effectively mobilize the resistance exerted by the shaft and carry the applied load. Based on the discussion of axial load changes along battered and vertical piles caused by the tunnel, it has been observed that there is an entirely different load transfer mechanism in battered piles. This mechanism varies not only with respect to depth of tunnel but also to the location of tunnel in relation to the batter of the pile.

3.3.2 Stress path evolution of the elements along the piles

To substantiate the discussion of load transfer mechanism of the battered and vertical piles during advancement of tunnelling, stress path evolution of selected elements at different depth along the pile length are computed. The three elements are at 2 m, 8 m and 17 m (i.e., underneath the pile toe) along the pile length. Figs. 8(a)-8(c) represent stress paths for selected elements at 2 m, 8 m and 17 depth m for each case of S_b, S_o, S_a and S_v, respectively. Furthermore, each figure includes the K_0 line, which represents coefficient of at-rest earth pressure, as well as the critical state line, serving as a point of reference. The initial stress state of all the chosen soil elements exhibits similarity and conforms to the K_0 stress condition, as anticipated. In the context of battered piles, the soil element located at a depth of 2 m (as seen in Fig. 8(a)) undergoes a rise in both the mean effective stress (p') and deviatoric stress (q upon the application of working load. The soil element situated at a depth of 2 m experiences compression as a result of the normal component of the applied load acting on the pile. The process of compression leads to a simultaneous increase of both the mean effective stress (p') and the deviatoric stress (q). After consolidation, p' and q continue to increase in each case. In the case of S_b, both p' and q increase significantly during advancement of tunnel. This is due to tunnelling-induced lateral load which leads to induce compression and shearing (compression loading) in the soil element. On the other, both q and p' decreased as tunnel passes the battered pile. The reason is attributed to the location of the tunnel being on other side of batter of the pile. As a result, the element is subjected to extension unloading due to development of lateral load. While the stress path of the element in case of S_a implies the compression loading and extension unloading response of the element during the tunnel excavation. When

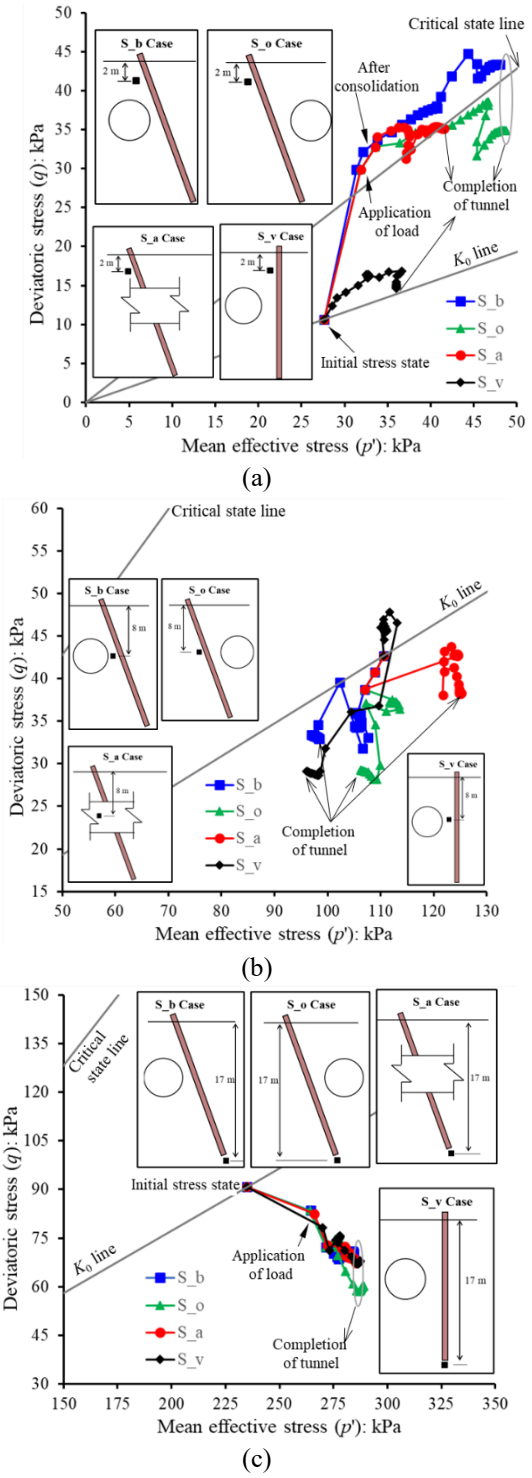

Fig. 8 Stress path evolution of the elements along the piles at different depths due to tunnelling below the pile toe (a) 2 m, (b) 8 m; and (c) 17 m

comparing the stress path of a soil element at a depth of 2 m in scenarios involving battered piles, it is observed that there is a minor rise in both the mean effective stress and the deviatoric stress in cases where the piles are oriented vertically. This is because shearing is induced in the soil element due to settlement caused by tunnelling. The element positioned at a vertical distance of 8 meters is situated between the pile and the springline of the tunnel, as depicted in Fig. 8(b). As the tunnel nears the pile, the elements undergo extension unloading caused by stress relief resulting from tunnelling in scenarios involving S_b and S_o. However, in the case of S_a, compression loading is induced in the soil element. The tunnel passes across the batter of the pile in case of S_a, causing development of

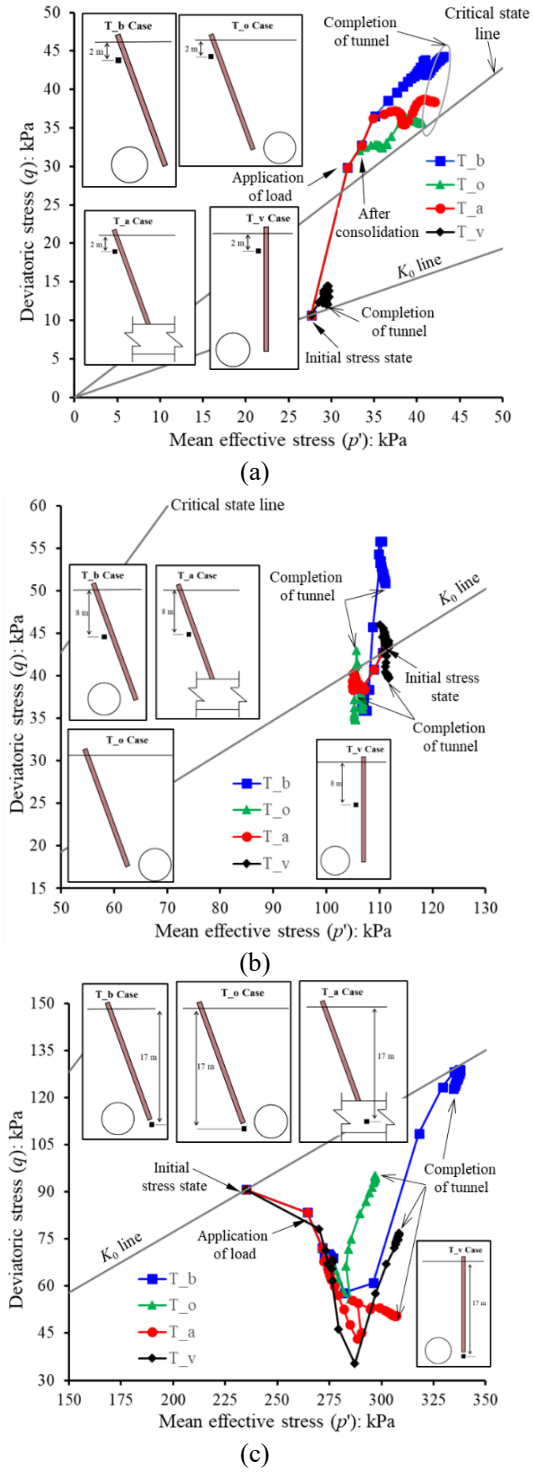

Fig. 9 Stress path evolution of the elements along the piles at different depths due to tunnelling next to the pile toe (a) 2 m, (b) 8 m; and (c) 17 m

lateral load in the pile which leads to an increment of the mean effective stress. As depicted in Fig. 8(c), the mean effective stress (p') exhibits an increase, while the deviatoric stress (q) experiences a decrease within the element situated underneath the pile toe, specifically at a depth of 17 m. This behaviour is observed across all scenarios, including S_b, S_o, S_a, and S_v. The occurrence of this phenomena can be attributed to the transfer of load from the shaft to the pile toe, which is a consequence of tunnelling activities.

Figs. 9(a)-9(c) represent stress paths for selected elements at depth of 2 m, 8 m and 17 m for each case of T_b, T_o, T_a and T_v, respectively. In cases of battered pile, both p' and q increase as the tunnel advances. The magnitude of the increment is highest for T_b and lowest for T_o. The development of lateral load in the pile, leading

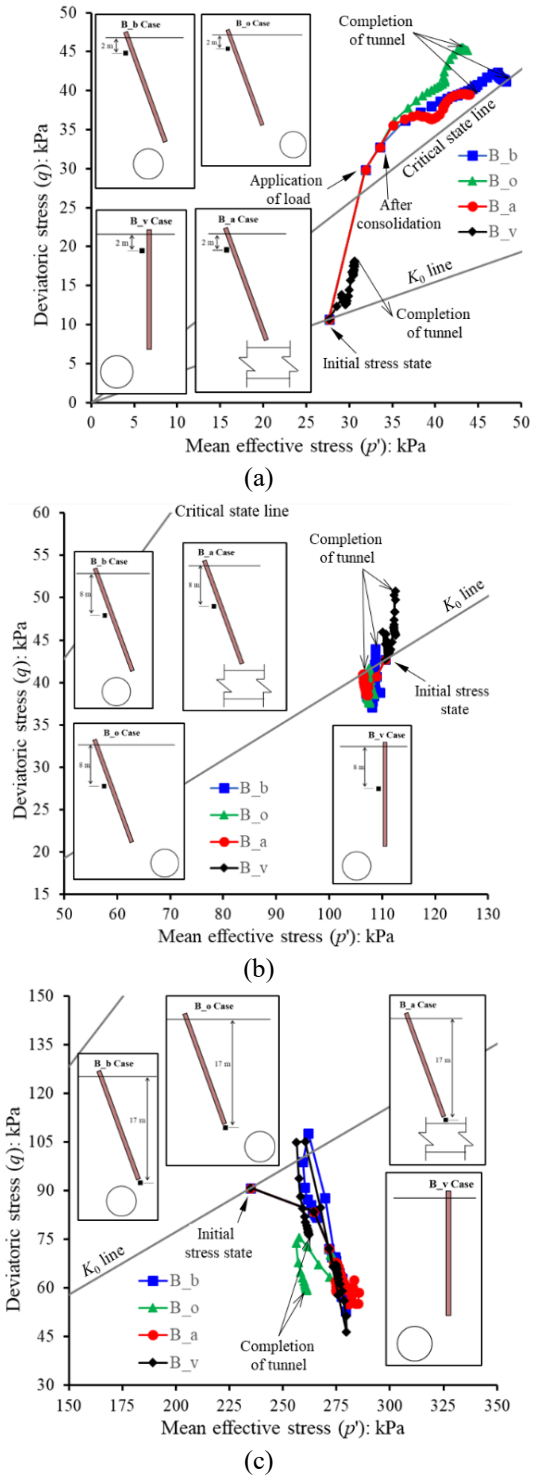

Fig. 10 Stress path evolution of the elements along the piles at different depths due to tunnelling below the pile toe (a) 2 m, (b) 8 m; and (c) 17 m

to compression of the soil element, can be attributed to the location of the tunnel on the batter side of the pile. Whereas the tunnel is excavated on the opposite side of the batter of the pile, which induces smaller lateral load in resulting in minimal magnitude of compression of the element. On the other hand, minimal changes in both p' and q occur in the element along the vertical pile (case of T_v). The element located at a depth of 8 m along the pile length is close to the tunnel in all cases, as shown in Fig. 9(b). As a result, the deviatoric stress (q) increases abruptly in the case of T_b, despite the constant mean effective stress (p'). This can be attributed to the combined effect of stress release caused by tunnelling and compression of the element due to lateral load . In case of T_o, the tunnel location being on the other

side of batter of the pile, q despite the constant p' increase slightly. Similar stress path is identified in case of T_a. On the other hand, the element along the vertical pile element at 8 m is subjected to reduction in the deviatoric stress with constant p' due to tunnelling. As shown in Fig. 12(c), the mean effective stress (p') increases and the deviatoric stress (q) decreases as the tunnel approaches the pile, but then rapidly increases after passing beyond the pile in all cases. The reason for this phenomenon can be attributed to the transmission of load from the shaft to the pile toe, as depicted in Fig. 10.

Figs. 10(a)-10(c) represent stress paths for selected elements at depth of 2 m, 8 m and 17 m for each case of B_b, B_o, B_a and B_v, respectively. In cases of battered pile, both p' and q increase as the tunnel advances. This is attributed to the location of the tunnel which is on the batter side of the pile in case of B_b resulting in lateral load in the pile resulting in compression of the soil element. The deviatoric stress slightly increases in the case of vertical piles (B_v). This can be attributed to the settlement of the pile, which mobilizes the shaft resistance (see Fig. 7) and causes shear within the element. As shown in Fig. 10(b), in cases of B_b, B_o and B_a, the deviatoric stress (q) decreases as the tunnel approaches the pile, but then rapidly increases after passing beyond the pile. On the other hand, the deviatoric stress (q) increases despite the constant mean effective stress (p') with in the soil element along the vertical pile in case of B_v. This can be attributed to the settlement of the pile, which mobilizes the shaft resistance (see Fig. 7) and causes shear within the element. In cases where the tunnel is excavated below the pile toe (B_b, B_o, B_a, and B_v as shown in Fig. 10(c)), there is a significant decrease in deviatoric stress within the element directly underneath the pile toe. This reduction in stress is caused by the stress resulting from tunnelling, which leads to decrease in end-bearing of the pile (see Fig. 7).

4. Conclusions

The paper examines the settlements and load changes that occur in a battered pile due to an adjacent tunnel excavation. The response of the battered pile is compared with that of a vertical pile. The study also includes parametric analyses to investigate the impact of various factors on the settlement of the adjacent battered pile, such as different tunnel depths in relation to the pile length, and the location of the tunnel in relation to the batter of the pile. Based on the results presented, the following conclusions can be drawn:

a) The settlement and load transfer mechanisms along the battered pile as a result of tunnelling are highly dependent on the location of the tunnel in relation to the batter, as well as the length of the pile. Furthermore, these mechanisms differ significantly from those observed in vertical piles during tunnelling. It was revealed that tunnelling activity near a battered pile is more vulnerable than that adjacent to a vertical pile.
b) The largest settlement of the battered pile is induced in case of T_o. This is due to significant stress relief affecting the lower part of the pile, including the pile toe, as a result of tunnelling near the pile toe during T_o. A wider zone of influence with respect to settlement (which is $-7.0 \leq y/D \leq +5.0$) is identified when the tunnel at different depths passes the pile across the battered position.
c) *py* curves (soil resistance and lateral deflection) curves are extensively utilized in the calculation of lateral pile capacity due to their ability to represent the nonlinear interaction between soil and pile. The tunnel excavated on the batter side of the pile results in an increase in both soil resistance and pile deflection, indicating that the pile is pushing against the soil and causing a passive loading state. Conversely, the movement of soil pushes the pile towards the tunnel which is excavated on the opposite of the batter of the pile, resulting in an active loading state. Furthermore, the behaviour of the *py* curves for vertical piles due to tunnelling is completely different from that of battered piles.
d) The battered pile is subjected to "dragload" due to negative skin friction mobilization due to tunnel excavation in cases of S_b, S_o and T_b. This occurs because the shaft of the battered pile experiences stress release due to tunnelling. Because the battered piles are installed at an angle, the surrounding soil settles more than the pile, causing it to be pulled downward and resulting in negative shaft resistance along the battered pile.

Acknowledgments

The authors would like to acknowledge the financial support provided China University of Mining and Technology, Xuzhou, China.

References

Benz, T. (2007), "Small-strain stiffness and its numerical consequences", Ph.D. thesis, Universität Stuttgart, Germany.

Bharathi, M., Dubey, R.N. and Shukla, S.K. (2022), "Numerical simulation of the dynamic response of batter piles and pile groups", *Bull. Earthq. Eng.*, **20**(7), 3239-3263. https://doi.org/10.1007/s10518-022-01362-7.

Boonsiri, I. and Takemura, J. (2015), "Observation of ground movement with existing pile groups due to tunneling in sand using centrifuge modelling", *Geotech. Geol. Eng.*, **33**, 621-640. https://doi.org/10.1007/s10706-015-9845-0.

Cheng, C.Y., Dasari, G.R., Chow, Y.K. and Leung, C.F. (2007), "Finite element analysis of tunnel-soil-pile interaction using displacement-controlled model", *Tunn. Undergr. Sp Tech.*, **22**, 450-466. https://doi.org/10.1016/j.tust.2006.08.002.

Coutts, D.R. and Wang, J. (2000), "Monitoring of reinforced concrete piles under horizontal and vertical loads", In *Proceeding of the International Conference on Tunnels and Underground Structures*, Singapore.

Ding, Z., Wei, X.J. and Wei, G. (2017), "Prediction methods on tunnel-excavation induced surface settlement around adjacent building", *Geomech. Eng.*, **12**(2), 185-195. https://doi.org/10.12989/gae.2017.12.2.185.

Franza, A. and Marshall, A.M. (2018), "Centrifuge modeling study of the response of piled structures to tunneling", *J. Geotech.*

Geoenviron. Eng., **144**(2), 04017109. https://doi.org/10.1061/(asce)gt.1943-5606.0001751.

Gasparre, A. (2005), "Advanced laboratory characterisation of London Clay", Ph.D. thesis, Dept. of Civil and Environmental Engineering, Univ. of London, UK.

Gu, W., Tong, L., Li, H. and Wu, K. (2023a), "A Numerical Study on the Lateral Pile–Soil Interaction During the Tunneling Process in Clay", *Iranian J. Sci. Tech. Transact. Civil Eng.*, 1-14.

Gu, W., Li, H. and Tong, L. (2023b), "Evaluation of tunneling-induced lateral pile response by an artificial intelligence optimization algorithm", *Int. J. Geomech.*, **23**(10), 04023178. https://doi.org/10.1061/ijgnai.gmeng-8685.

Hibbitt, Karlsson, Sorensen. (2015), *Abaqus user's manual, version 6.14-2*. Providence, RI, USA: Hibbitt, Karlsson and Sorensen Inc.

Hong, Y., Soomro, M.A. and Ng, C.W.W. (2015), "Settlement and load transfer mechanism of pile group due to side-by-side twin tunnelling", *Computers and Geotechnics*, **64**, 105-119. https://doi.org/10.1016/j.compgeo.2014.10.007.

Jacobsz, S.W., Bowers, K.H., Moss, N.A. and Zanardo, G. (2006), "The effects of tunnelling on piled structures on the CTRL. In: Geotechnical aspects of underground construction in soft ground", *Proceedings of the 5th international symposium TC28*, Amsterdam, the Netherlands, 15-17 June 2005.

Jamil, I. and Ahmad, I. (2019), "Bending moments in raft of a piled raft system using Winkler analysis", *Geomech. Eng.*, **18**(1), 41-48. https://doi.org/10.12989/gae.2019.18.1.041.

Karira, H., Kumar, A., Ali, T.H., Mangnejo, D.A. and Mangi, N. (2022), "A parametric study of settlement and load transfer mechanism of piled raft due to adjacent excavation using 3D finite element analysis", *Geomech. Eng.*, **30**(2), 169-185. https://doi.org/10.12989/gae.2022.30.2.169.

Lee, G.T.K. and Ng, C.W.W. (2005), "The effects of advancing open face tunneling on an existing loaded pile", *J. Geotech. Geoenviron. Eng. - ASCE*, **131**, 193-201. https://doi.org/10.1061/(asce)1090-0241(2005)131:2(193).

Lee, S.W. (2019), "Experimental study on effect of underground excavation distance on the behavior of retaining wall", *Geomech. Eng.*, **17**(5), 413-420. https://doi.org/10.12989/gae.2019.17.5.413.

Loganathan, N., Poulos, H.G. and Stewart, D.P. (2000), "Centrifuge model testing of tunnelling-induced ground and pile deformations", *Géotechnique*, **50**, 283-294. https://doi.org/10.1680/geot.2000.50.3.283.

Lu, H., Shi, J., Ng, C.W.W. and Lv, Y. (2020), "Three-dimensional centrifuge modeling of the influence of side-by-side twin tunneling on a piled raft", *Tunn. Undergr. Sp. Tech.*, **103**, 103486. https://doi.org/10.1016/j.tust.2020.103486.

Mair, R.J. and Taylor, R.N. (1997), "Bored tunnelling in the urban environment. state-of-the-art report and theme lecture", *Proceedings of 14th International Conference on Soil Mechanics and Foundation Engineering, Hamburg*, Balkema.

Mašín, D. (2005), "A hypoplastic constitutive model for clays", *Int. J. Numer. Anal. Meth. Geomech.*, **29**(4), 311-336. https://doi.org/10.1002/nag.416.

Mašín, D. and Herle, I. (2005), "State boundary surface of a hypoplastic model for clays", *Comput. Geotech.*, **32**(6), 400-410. https://doi.org/10.1016/j.compgeo.2005.09.001.

Meguid, M.A., Saada, O., Nunes, M.A. and Mattar, J. (2008), "Physical modeling of tunnels in soft ground: a review", *Tunn. Undergr. Sp. Tech.*, **23**(2), 185-198. https://doi.org/10.1016/j.tust.2007.02.003.

Mu, L., Huang, M., Roodi, G.H. and Shi, Z. (2021), "Allowable wall deflection of braced excavation adjacent to pile-supported buildings", *Geomech. Eng.*, **26**(2), 161-173. https://doi.org/10.12989/gae.2021.26.2.161.

Ng, C.W.W., Lu, H. and Peng, S.Y. (2013), "Three-dimensional centrifuge modelling of effects of twin tunnelling on as existing pile", *Tunn. Undergr. Sp. Tech.*, **35**, 189-199. https://doi.org/10.1016/j.tust.2012.07.008.

Ng, C.W.W., Soomro, M.A. and Hong, Y. (2014), "Three-dimensional centrifuge modelling of pile group responses to side-by-side twin tunnelling", *Tunn. Undergr. Sp. Tech.*, **43**, 350-361. https://doi.org/10.1016/j.tust.2014.05.002.

Ng, C.W.W., Hong, Y. and Soomro, M.A. (2015), "Effects of piggyback twin tunnelling on a pile group: 3D centrifuge tests and numerical modelling", *Géotechnique*, **65**(1), 38-51. https://doi.org/10.1680/geot.14.p.105.

Niemunis, A. and Herle, I. (1997), "Hypoplastic model for cohesionless soils with elastic strain range", *Mech. Cohesive-Frict. Mater*, **2**, 279-299.

Qian, J., Tong, Y., Mu, L., Lu, Q. and Zhao, H. (2020), "A displacement-controlled method for evaluating ground settlement induced by excavation in clay", *Geomech. Eng.*, **20**(4), 275-285. https://doi.org/10.12989/gae.2020.20.4.275.

Shi, J., Wei, J., Ng, C.W.W. and Lu, H. (2019), "Stress transfer mechanisms and settlement of a floating pile due to adjacent multi-propped deep excavation in dry sand", *Comput. Geotech.*, **116**, 103216. https://doi.org/10.1016/j.compgeo.2019.103216.

Shirlaw, J.N., Ong, J.C.W., Rosser, H.B., Tan, C.G., Osborne, N. H. and Heslop, P.E. (2003), "Local settlements and sinkholes due to EPB tunnelling", *Geotech. Eng.*, **156**(4), 193-211. https://doi.org/10.1680/geng.156.4.193.37533.

Soomro, M.A., Mangi, N., Cheng, W.C. and Mangnejo, D.A. (2020), "The effects of multipropped deep excavation-induced ground movements on adjacent high-rise building founded on piled raft in sand", *Adv. Civil Eng.*, **2020**(1), 8897507. https://doi.org/10.1155/2020/8897507.

Soomro, M.A., Kumar, M., Mangi, N., Mangnejo, D.A. and Cui, Z.D. (2022a), "Parametric study of twin tunneling effects on piled foundations in stiff clay: 3D finite-element approach", *Int. J. Geomech.*, **22**(6), 04022079. https://doi.org/10.1061/(ASCE)GM.1943-5622.000238.

Soomro, M.A., Mangi, N., Memon, A.H. and Mangnejo, D.A. (2022b), "Responses of high-rise building resting on piled raft to adjacent tunnel at different depths relative to piles", *Geomech. Eng.*, **29**(1), 25-40. https://doi.org/10.12989/gae.2022.29.1.025.

Soomro, M.A., Mangi, N., Mangnejo, D.A. and Zhang, Z. (2023), "The responses of battered pile to tunnelling at different depths relative to the pile length", *Geomech. Eng.*, **35**(6), 603-615. https://doi.org/10.12989/gae.2023.35.6.603.

Soomro, M.A., Liu, K., Cui, Z.D., Mangi, N. and Mangnejo, D.A. (2024a), "Insights from 3D numerical simulations on the impact of tunnelling on vertical and battered pile groups under lateral loading", *Comput. Geotech.*, **169**, 106195. https://doi.org/10.1016/j.compgeo.2024.106195.

Soomro, M.A., Mangi, N., Cui, Z.D., Liu, K. and Mangnejo, D.A. (2024b), "Evaluation of response mechanisms in an elevated pile group subjected to lateral loading caused by twin-tunnelling", *Comput. Geotech.*, **171**, 106334. https://doi.org/10.1016/j.compgeo.2024.106334.

Xu, J.M., Wang, C.C., Cheng, Z.L., Xu, T., Zhang, D.W. and Li, Z.L. (2024), "Intelligent prediction model of tunnelling-induced building deformation based on genetic programming and its application", *J. Central South Univ.*, 1-15. https://doi.org/10.1007/s11771-024-5656-x.

Xu, J., Yu, Z., Chen, R., Xu, T., Chen, C. and Wang, Z. (2025a), "Evaluation of the shear stiffness and load redistribution of framed structures affected by tunnelling", *Comput. Geotech.*, **177**, 106899. https://doi.org/10.1016/j.compgeo.2024.106899.

Xu, J., Zheng, L., Yu, Z., Li, Y. and Cai, G. (2025b), "Effects of bending stiffness and interface roughness on tunnel-embedded

wall interaction", *Tunn. Undergr. Sp. Tech.*, **155**, 106209. https://doi.org/10.1016/j.tust.2024.106209.

Zhang, R.J., Zheng, J.J., Zhang, L.M. and Pu, H.F. (2011), "An analysis method for the influence of tunneling on adjacent loaded pile groups with rigid elevated caps", *Int. J. Numer. Anal. Method. Geomech*., **35**(18), 1949-1971. https://doi.org/10.1002/nag.989.

CC